Journal of Zhejiang University-SCIENCE C (Computers & Electronics)
ISSN 1869-1951 (Print); ISSN 1869-196X (Online)
www.zju.edu.cn/jzus; www.springerlink.com
E-mail: jzus@zju.edu.cn

# Visual salience guided feature-aware shape simplification*

Yong-wei MIAO†[1], Fei-xia HU[1], Min-yan CHEN[1], Zhen LIU[2], Hua-hao SHOU[2]

([1]*College of Computer Science and Technology, Zhejiang University of Technology, Hangzhou 310023, China*)

([2]*College of Science, Zhejiang University of Technology, Hangzhou 310023, China*)

†E-mail: ywmiao@zjut.edu.cn

Received Mar. 18, 2014; Revision accepted July 26, 2014; Crosschecked Aug. 19, 2014

**Abstract:** In the area of 3D digital engineering and 3D digital geometry processing, shape simplification is an important task to reduce their requirement of large memory and high time complexity. By incorporating the content-aware visual salience measure of a polygonal mesh into simplification operation, a novel feature-aware shape simplification approach is presented in this paper. Owing to the robust extraction of relief heights on 3D highly detailed meshes, our visual salience measure is defined by a center-surround operator on Gaussian-weighted relief heights in a scale-dependent manner. Guided by our visual salience map, the feature-aware shape simplification algorithm can be performed by weighting the high-dimensional feature space quadric error metric of vertex pair contractions with the weight map derived from our visual salience map. The weighted quadric error metric is calculated in a six-dimensional feature space by combining the position and normal information of mesh vertices. Experimental results demonstrate that our visual salience guided shape simplification scheme can adaptively and effectively re-sample the underlying models in a feature-aware manner, which can account for the visually salient features of the complex shapes and thus yield better visual fidelity.

**Key words:** Visual salience, Shape simplification, Content-aware, Weighted quadric error metric, Feature-aware
**doi:**10.1631/jzus.C1400097 **Document code:** A **CLC number:** TP391.7

## 1 Introduction

Large scale sampled data of complex highly detailed shapes always exhibits a large proportion of redundant information due to the uniform sampling of common 3D automatic scanning devices (Luebke *et al.*, 2003; Botsch *et al.*, 2007). Such complex 3D models often incur some difficulties due to their requirement of large memory and high time complexity in both shape modeling and real-time rendering (Luebke, 2001; Luebke *et al.*, 2003), such as rapid prototype reconstruction in industry design, remote transmission in virtual reality, and real-time performance in digital entertainment. To overcome these difficulties, shape simplification and re-sampling schemes provide some efficient solutions for shape modeling and rendering tasks (Luebke, 2001; Xiao *et al.*, 2009; Miao *et al.*, 2012a; 2012b). In particular, feature-aware shape simplification techniques satisfy the need for maintaining intrinsic shape features with high visual fidelity during the data reducing operation (van Kaick and Pedrini, 2006).

By incorporating the visual salience measure into the shape re-sampling operation, a novel salience guided mesh simplification technique is presented in this paper. The relief heights of complex shapes are extracted robustly, and the content-aware visual salience map can then be calculated in a scale-dependent manner using a center-surround operator on Gaussian-weighted relief heights. Guided by our salience measure, the adaptive mesh re-sampling can be performed during a series of vertex pair collapse operations.

The main contribution of our work is that a novel feature-aware shape simplification scheme is presented by pushing the influence of our content-aware visual importance into the iterative contractions of

* Project supported by the National Natural Science Foundation of China (No. 61272309) and the Key Laboratory of Visual Media Intelligent Process Technology of Zhejiang Province, China (No. 2011E10003)

vertex pairs, which yields simplified models with high visual fidelity. We measure the contraction error by the salience-weighted quadric error metric, which is calculated in a six-dimensional (6D) feature space. The feature space will combine the position and normal information of mesh vertices. Compared to traditional simplification approaches (Garland and Heckbert, 1997; Luebke, 2001), the final distribution of sampled vertices generated by our re-sampling scheme will be guided by the visual perceptual properties and thus reflect the visually salient feature regions of the underlying models.

## 2 Related work

Here, we review some related work about shape simplification and re-sampling, especially the error metric based techniques using a diverse set of error metrics (Luebke, 2001; van Kaick and Pedrini, 2006).

Some classical shape simplification techniques take the geometric distance error of the simplified surface to the original one as a quality measure of shape fidelity to guide the re-sampling operation. Hoppe *et al.* (1993) first presented an edge contraction operation to simplify the given shape using an energy function to measure the simplification quality. Extending from this work, combining the colors, normal, and texture coordinates into the simplification error definition, Hoppe (1996) further proposed a progressive mesh representation scheme in the application of progressive transmission for 3D polygonal models. To restrict the maximum decimation error during the shape simplification procedure, Cohen *et al.* (1996) gave an error-controllable re-sampling scheme by limiting the simplified model between two additional inner and outer envelopes. As a classical vertex pair contraction based simplification scheme, the QSlim algorithm introduced by Garland and Heckbert (1997) uses a quadric error metric to evaluate the cost of edge contraction. The quadric error metric measures the sum of the squared distances from a vertex to the planes of neighboring triangles and can be represented as a symmetric 4×4 matrix. Extending from the pure geometric error metric, Garland and Heckbert (1998) presented a generalized quadratic error metric to simplify surfaces with vertex properties such as vertex color and texture. Furthermore, Hoppe (1999) described a new quadric error metric for simplifying meshes with appearance attributes. Wu *et al.* (2004) introduced a modified quadratic error metric to define the edge contraction cost for preserving the global geometric features during shape re-sampling. Based on the feature sensitive metric of polygonal meshes, Wei and Lou (2010) also presented a feature-preserving simplification approach by extending the quadric error to a high-dimensional feature-sensitive metric space.

However, due to their lack of visual perception considerations during shape simplification and re-sampling, most of these proposed algorithms could lose some visually salient features of 3D complex shapes and may induce visual degeneration after a drastic simplification (Fleming and Singh, 2009).

By incorporating the human visual system and perception theory (Itti *et al.*, 1998; Todd, 2004; Corsini *et al.*, 2013) into shape simplification applications, many perceptually driven surface re-sampling approaches have been presented in the area of computer graphics. Owing to the psychophysical model of visual perception, Luebke and Hallen (2001) presented a perceptually driven simplification scheme for interactive mesh rendering. Their work can also be extended to simplify a much broader class of models by accounting for textures and dynamic lighting (Williams *et al.*, 2003). Lee *et al.* (2005) introduced a bottom-up definition of mesh saliency to measure the region importance of meshes and also presented a saliency-based mesh simplification scheme. Its effectiveness has been shown by incorporating mesh saliency into shape re-sampling (Howlett *et al.*, 2005). Qu and Meyer (2008) integrated the visual masking importance measure of visual patterns on the underlying shape into the geometry-based QSlim simplification algorithm (Garland and Heckbert, 1997), which makes the approximation error less visible in areas of a strong visual masking map. Recently, combining the simple visual importance measure defined by vertex curvature entropy and the traditional quadric error metric, Xing and Hui (2012) presented a visual and geometry-based hybrid approach for surface simplification, which could produce a simplified model closer to the original one according to visual similarity.

The above approaches can generate simplified meshes with some interesting features; however, they do not consider the preservation of fine-scale relief

details of 3D complex shapes with a lot of meso-structures during the re-sampling operation. For complex relief surfaces, a novel content-aware visual salience measure is defined in this paper to reflect their visually distinctive relief details, and a feature-aware simplification technique is presented for polygonal meshes by weighting the feature space quadric error metric of vertex pair contractions with a visual perceptual measure.

## 3 Content-aware visual salience measure

For highly detailed 3D shapes, the abundant geometric details, called in the literature relief textures or surface meso-structures, can always effectively guide the viewer's visual attention in low-level human vision (Shilane and Funkhouser, 2007; Miao *et al.*, 2012b; Corsini *et al.*, 2013). For relief surfaces, Miao *et al.* (2012b) gave a definition of the multi-channel salience measure by combining three feature maps, i.e., the 0-order feature map of local height distribution, the 1-order feature map of normal difference, and the 2-order feature map of mean curvature variation. Different from the existing definitions of mesh saliency (Lee *et al.*, 2005; Liu *et al.* 2007), a novel content-aware salience measure for complex relief shapes is presented here using a center-surround operator on Gaussian-weighted relief heights in a scale-dependent manner.

Given a complex polygonal model $S$ (always represented as a triplet $S=\{V; E; F\}$ of vertices $V$, edges $E$, and facets $F$), the relief height $h(\boldsymbol{v})$ of each vertex $\boldsymbol{v}\in V$ could be determined implicitly using Zatzarinni *et al*. (2009)'s indirect approach. That is, the relief height values can be estimated by minimizing the energy function:

$$\min_{h(\boldsymbol{v}_i),\, i=1,2,\ldots,n} \sum_{\boldsymbol{e}_{ij}\in E} \left[ h(\boldsymbol{v}_i) - h(\boldsymbol{v}_j) - \Delta h(\boldsymbol{e}_{ij}) \right]^2. \quad (1)$$

Here, $n$ is the number of model vertices. The energy function (1) can be solved using the conjugate gradient method (Press *et al.*, 1992). Here, the height difference $\Delta h(\boldsymbol{e}_{ij})$ between two neighboring vertices can be calculated as the projection of the edge $(\boldsymbol{v}_i, \boldsymbol{v}_j)=\boldsymbol{e}_{ij}\in E$ onto their average normal, that is, $\Delta h(\boldsymbol{e}_{ij})=(\boldsymbol{v}_i-\boldsymbol{v}_j)\boldsymbol{N}_{\mathrm{B}}(\boldsymbol{e}_{ij})$, where

$$\boldsymbol{N}_{\mathrm{B}}(\boldsymbol{e}_{ij}) = \left(\boldsymbol{N}_{\mathrm{B}}(\boldsymbol{v}_i) + \boldsymbol{N}_{\mathrm{B}}(\boldsymbol{v}_j)\right) \Big/ \| \boldsymbol{N}_{\mathrm{B}}(\boldsymbol{v}_i) + \boldsymbol{N}_{\mathrm{B}}(\boldsymbol{v}_j) \|.$$

The base normal $\boldsymbol{N}_{\mathrm{B}}(\boldsymbol{v})$ for each vertex $\boldsymbol{v}$ can be simply calculated using the normalized average normal of the base surface for its incident faces, which can be obtained using Ohtake *et al.* (2002)'s anisotropic Gaussian mesh filtering scheme.

Owing to the estimated relief height distribution, our content-aware mesh salience measure of each vertex can be defined using the center-surround mechanism on surface relief height distribution on multiple scales. In our experiments, we first search for the neighboring vertices $\boldsymbol{x}$ within a radius of $2\sigma$ at each vertex $\boldsymbol{v}$ and calculate the Gaussian-weighted average of the relief height $h(\boldsymbol{x})$ as follows:

$$G(h(\boldsymbol{v}),\sigma) = \frac{\sum_{\boldsymbol{x}\in N(\boldsymbol{v},2\sigma)} h(\boldsymbol{x}) \exp(-\| \boldsymbol{x}-\boldsymbol{v} \|^2 / (2\sigma^2))}{\sum_{\boldsymbol{x}\in N(\boldsymbol{v},2\sigma)} \exp(-\| \boldsymbol{x}-\boldsymbol{v} \|^2 / (2\sigma^2))}. \quad (2)$$

Thus, the single-scale salience measure of vertex $\boldsymbol{v}$ is calculated as the absolute difference between the fine-scale Gaussian-weighted average and the coarse scale one, that is,

$$\zeta(\boldsymbol{v}) = \left| G(h(\boldsymbol{v}),\sigma) - G(h(\boldsymbol{v}),2\sigma) \right|. \quad (3)$$

To estimate the content-aware mesh salience on multiple scales, we denote the vertex salience of vertex $\boldsymbol{v}$ at scale level $i$ as $\zeta_i(\boldsymbol{v})$ with the standard deviation of the Gaussian filter $\sigma_i$. Similar to Lee *et al.* (2005), we use five scales $\sigma_i\in\{2\varepsilon, 3\varepsilon, 4\varepsilon, 5\varepsilon, 6\varepsilon\}$ to evaluate the mesh salience of different scales, and in our practice $\varepsilon$ is 0.15% of the diagonal length of the bounding box for the underlying model. Finally, our content-aware salience measure $s(\boldsymbol{v})$ of each vertex $\boldsymbol{v}$ can be estimated by adding the salience maps at all five scales after applying nonlinear normalization of suppression.

Fig. 1 gives our content-aware salience estimation and its comparison with the traditional salience measure for the Mountain relief model (Fig. 1a). The relief height map is first extracted for different complex shapes, and our content-aware salience map can thus be calculated using the center-surround mechanism on surface relief height distribution at multiple

scales (Fig. 1b). Fig. 2 also shows some examples to compare our salience map with the traditional salience measure for Horse, Stanford Bunny, and Lion models. Figs. 1c and 2c show Lee *et al.* (2005)'s mesh saliency estimations, and Figs. 1d and 2d show Liu *et al.* (2007)'s mesh saliency measure for different models. In contrast to Lee *et al.* (2005) and Liu *et al.* (2007)'s mesh saliency definitions, our content-aware salience map can effectively illustrate the visually salient geometric details and highlight some meso-structures of underlying relief shapes that always attract the viewers' visual attention.

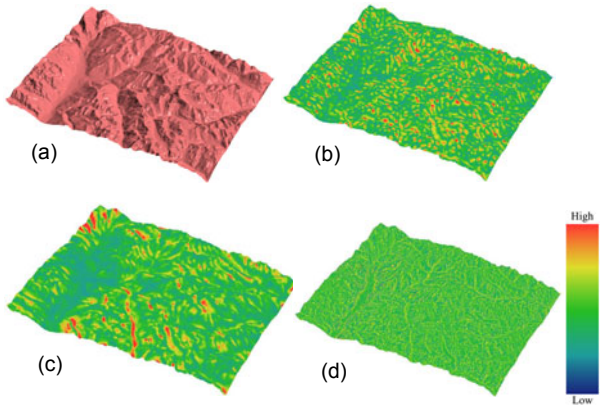


**Fig. 1 Visual salience map for the Mountain relief model**
(a) Original model; (b) Our salience map; (c) Lee *et al.* (2005)'s salience map; (d) Liu *et al.* (2007)'s salience map

## 4 Visual salience guided shape simplification

### 4.1 Motivation of our simplification scheme

As an effective measure of low-level human visual attention, our proposed visual salience map of complex shapes can influence which part of a given model the user will look at and pay more attention to. Obviously, these visually salient surface regions should be effectively preserved by introducing smaller simplification errors and achieve high visual fidelity during the shape re-sampling operation. However, the visually less important regions could be simplified and represented by few triangles to satisfy the rate of the simplification budget, because the simplification error in these regions will be less noticed by the user.

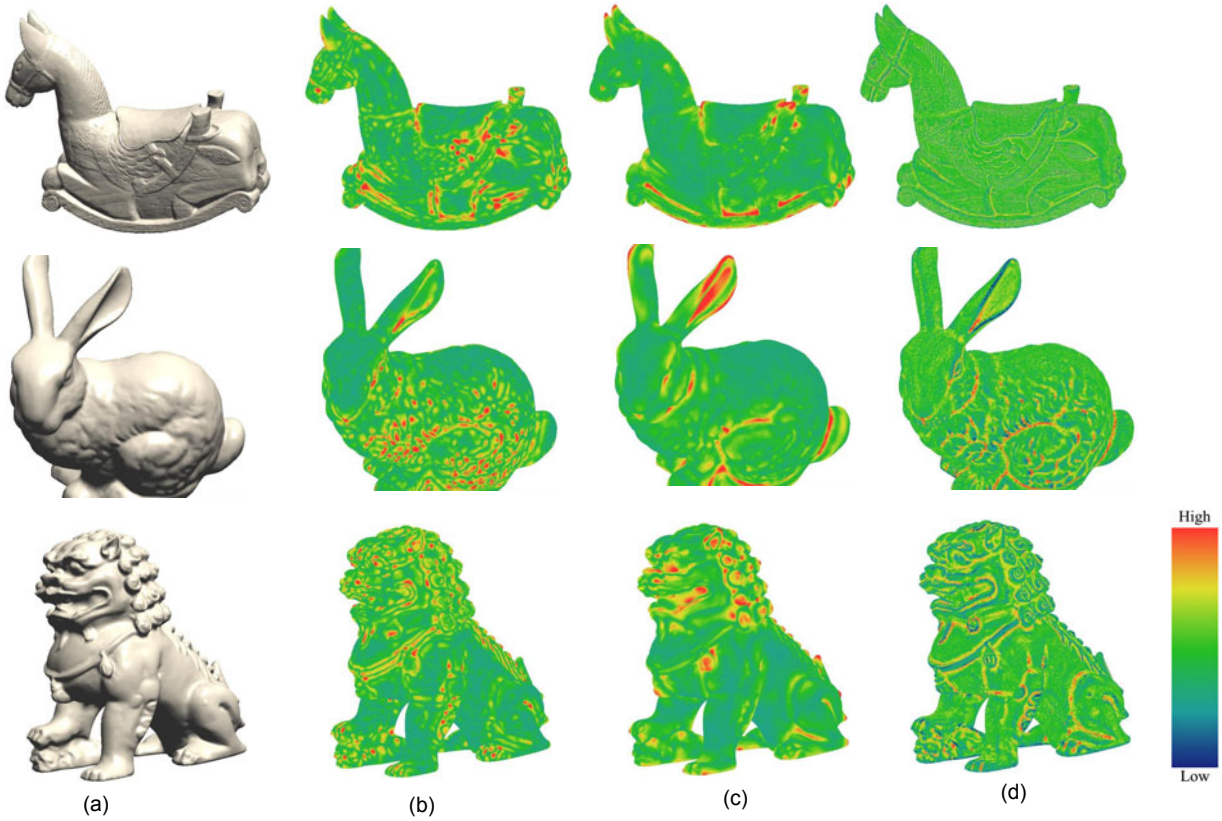


**Fig. 2 Visual salience map for Horse, Stanford Bunny, and Lion models**
(a) Original model; (b) Our salience map; (c) Lee *et al.* (2005)'s salience map; (d) Liu *et al.* (2007)'s salience map

Here, our content-aware salience map is introduced as an importance measure of relief mesostructures for complex shapes, and a salience guided shape simplification scheme can be performed by weighting the high-dimensional feature space quadric error metric of the vertex pair contractions with our visual salience measure.

### 4.2 Visual salience guided feature-aware simplification

By incorporating our content-aware visual salience map of complex models into the re-sampling operation, a feature-aware shape simplification technique is presented here. In contrast to the traditional QSlim simplification method (Garland and Heckbert, 1997), we place the surface vertices in a 6D feature space by combining their position and normal information. The reason for exploiting the 6D feature space is that the variations of both vertex positions and normal directions reflect the intrinsic geometric features and thus can be regarded as a cue to guide the adaptive vertex distribution of the simplified models with high visual fidelity.

For each vertex $\boldsymbol{v}$ of a given 3D complex model $S$, its 6D feature point can be represented as $\bar{\boldsymbol{v}}=(v_x, v_y, v_z, n_x, n_y, n_z)^{\mathrm{T}}$, which combines its position information $(v_x, v_y, v_z)$ and normal information $(n_x, n_y, n_z)$. For each triangular facet $\Delta=(\boldsymbol{p}, \boldsymbol{q}, \boldsymbol{r})$ of the original model, a corresponding 2D super-plane $\bar{\Delta}=(\bar{\boldsymbol{p}}, \bar{\boldsymbol{q}}, \bar{\boldsymbol{r}})$ can be obtained in the 6D feature space and an orthonormal basis of the 2D super-plane can thus be constructed. For example, we set $\bar{\boldsymbol{p}}$ as the origin of coordinates in the 6D feature space, $\bar{\boldsymbol{e}}_1$ a unit vector along direction $\overline{\boldsymbol{pq}}$, and $\bar{\boldsymbol{e}}_2$ the orthonormal unit vector of $\bar{\boldsymbol{e}}_1$ (Fig. 3).

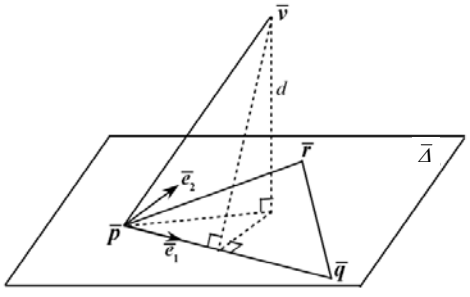


**Fig. 3 Computation of the squared distance of a vertex to the 2D super-plane**

According to the quadric error metric analysis (Garland and Heckbert, 1997; 1998), the high dimensional quadric error metric can be determined as the squared distance of vertex $\bar{\boldsymbol{v}}$ to the 2D super-plane $\bar{\Delta}=(\bar{\boldsymbol{p}}, \bar{\boldsymbol{q}}, \bar{\boldsymbol{r}})$ (Fig. 3), that is,

$$\begin{aligned}
&D^2(\bar{\boldsymbol{v}},\bar{\Delta})=d^2=\|\bar{\boldsymbol{v}}-\bar{\boldsymbol{p}}\|^2-[(\bar{\boldsymbol{v}}-\bar{\boldsymbol{p}})^{\mathrm{T}}\bar{\boldsymbol{e}}_1]^2-[(\bar{\boldsymbol{v}}-\bar{\boldsymbol{p}})^{\mathrm{T}}\bar{\boldsymbol{e}}_2]^2\\
&=(\bar{\boldsymbol{v}}^{\mathrm{T}}-\bar{\boldsymbol{p}}^{\mathrm{T}})(\bar{\boldsymbol{v}}-\bar{\boldsymbol{p}})-(\bar{\boldsymbol{v}}^{\mathrm{T}}-\bar{\boldsymbol{p}}^{\mathrm{T}})\bar{\boldsymbol{e}}_1\bar{\boldsymbol{e}}_1^{\mathrm{T}}(\bar{\boldsymbol{v}}-\bar{\boldsymbol{p}})\\
&\quad-(\bar{\boldsymbol{v}}^{\mathrm{T}}-\bar{\boldsymbol{p}}^{\mathrm{T}})\bar{\boldsymbol{e}}_2\bar{\boldsymbol{e}}_2^{\mathrm{T}}(\bar{\boldsymbol{v}}-\bar{\boldsymbol{p}})\\
&=\bar{\boldsymbol{v}}^{\mathrm{T}}(\boldsymbol{I}-\bar{\boldsymbol{e}}_1\bar{\boldsymbol{e}}_1^{\mathrm{T}}-\bar{\boldsymbol{e}}_2\bar{\boldsymbol{e}}_2^{\mathrm{T}})\bar{\boldsymbol{v}}-2\bar{\boldsymbol{p}}^{\mathrm{T}}(\boldsymbol{I}-\bar{\boldsymbol{e}}_1\bar{\boldsymbol{e}}_1^{\mathrm{T}}-\bar{\boldsymbol{e}}_2\bar{\boldsymbol{e}}_2^{\mathrm{T}})\bar{\boldsymbol{v}}\\
&\quad+\bar{\boldsymbol{p}}^{\mathrm{T}}(\boldsymbol{I}-\bar{\boldsymbol{e}}_1\bar{\boldsymbol{e}}_1^{\mathrm{T}}-\bar{\boldsymbol{e}}_2\bar{\boldsymbol{e}}_2^{\mathrm{T}})\bar{\boldsymbol{p}}\\
&=\bar{\boldsymbol{v}}^{\mathrm{T}}(\boldsymbol{I}-\bar{\boldsymbol{e}}_1\bar{\boldsymbol{e}}_1^{\mathrm{T}}-\bar{\boldsymbol{e}}_2\bar{\boldsymbol{e}}_2^{\mathrm{T}})\bar{\boldsymbol{v}}+2[(\bar{\boldsymbol{p}}^{\mathrm{T}}\cdot\bar{\boldsymbol{e}}_1)\bar{\boldsymbol{e}}_1+(\bar{\boldsymbol{p}}^{\mathrm{T}}\cdot\bar{\boldsymbol{e}}_2)\bar{\boldsymbol{e}}_2-\bar{\boldsymbol{p}}]^{\mathrm{T}}\bar{\boldsymbol{v}}\\
&\quad+\bar{\boldsymbol{p}}^{\mathrm{T}}\cdot\bar{\boldsymbol{p}}-(\bar{\boldsymbol{p}}^{\mathrm{T}}\cdot\bar{\boldsymbol{e}}_1)^2-(\bar{\boldsymbol{p}}^{\mathrm{T}}\cdot\bar{\boldsymbol{e}}_2)^2.
\end{aligned}$$

Thus, we have the following formula for the error metric:

$$D^2(\bar{\boldsymbol{v}},\bar{\Delta})=\bar{\boldsymbol{v}}^{\mathrm{T}}\boldsymbol{A}(\bar{\boldsymbol{v}},\bar{\Delta})\bar{\boldsymbol{v}}+2\boldsymbol{b}(\bar{\boldsymbol{v}},\bar{\Delta})^{\mathrm{T}}\bar{\boldsymbol{v}}+c(\bar{\boldsymbol{v}},\bar{\Delta}). \quad (4)$$

The error triplet in Eq. (4) can be calculated as

$$\begin{cases}
\boldsymbol{A}(\bar{\boldsymbol{v}},\bar{\Delta})=\boldsymbol{I}-\bar{\boldsymbol{e}}_1\bar{\boldsymbol{e}}_1^{\mathrm{T}}-\bar{\boldsymbol{e}}_2\bar{\boldsymbol{e}}_2^{\mathrm{T}},\\
\boldsymbol{b}(\bar{\boldsymbol{v}},\bar{\Delta})=(\bar{\boldsymbol{p}}^{\mathrm{T}}\cdot\bar{\boldsymbol{e}}_1)\bar{\boldsymbol{e}}_1+(\bar{\boldsymbol{p}}^{\mathrm{T}}\cdot\bar{\boldsymbol{e}}_2)\bar{\boldsymbol{e}}_2-\bar{\boldsymbol{p}},\\
c(\bar{\boldsymbol{v}},\Delta)=\bar{\boldsymbol{p}}^{\mathrm{T}}\cdot\bar{\boldsymbol{p}}-(\bar{\boldsymbol{p}}^{\mathrm{T}}\cdot\bar{\boldsymbol{e}}_1)^2-(\bar{\boldsymbol{p}}^{\mathrm{T}}\cdot\bar{\boldsymbol{e}}_2)^2.
\end{cases} \quad (5)$$

The final error metric of vertex $\boldsymbol{v}$ can be defined as the weighted sum of the quadric errors to its associated 2D neighboring super-plane set:

$$\begin{aligned}
\mathrm{Error}(v)&=\bar{\boldsymbol{v}}^{\mathrm{T}}\boldsymbol{A}(\bar{\boldsymbol{v}})\bar{\boldsymbol{v}}+2\boldsymbol{b}(\bar{\boldsymbol{v}})^{\mathrm{T}}\bar{\boldsymbol{v}}+c(\bar{\boldsymbol{v}})\\
&=\sum_{\bar{\Delta}}D^2(\bar{\boldsymbol{v}},\bar{\Delta})\mathrm{Area}(\bar{\Delta})\Big/\sum_{\bar{\Delta}}\mathrm{Area}(\bar{\Delta}).
\end{aligned} \quad (6)$$

For convenience, we represent the quadric error metric as triplet $\mathrm{Error}(\boldsymbol{v})=(\boldsymbol{A}(\bar{\boldsymbol{v}}),\boldsymbol{b}(\bar{\boldsymbol{v}}),c(\bar{\boldsymbol{v}}))$, where

$$\begin{cases}
\boldsymbol{A}(\bar{\boldsymbol{v}})=\sum_{\bar{\Delta}}\boldsymbol{A}(\bar{\boldsymbol{v}},\bar{\Delta})\mathrm{Area}(\bar{\Delta})\Big/\sum_{\bar{\Delta}}\mathrm{Area}(\bar{\Delta}),\\
\boldsymbol{b}(\bar{\boldsymbol{v}})=\sum_{\bar{\Delta}}\boldsymbol{b}(\bar{\boldsymbol{v}},\bar{\Delta})\mathrm{Area}(\bar{\Delta})\Big/\sum_{\bar{\Delta}}\mathrm{Area}(\bar{\Delta}),\\
c(\bar{\boldsymbol{v}})=\sum_{\bar{\Delta}}c(\bar{\boldsymbol{v}},\bar{\Delta})\mathrm{Area}(\bar{\Delta})\Big/\sum_{\bar{\Delta}}\mathrm{Area}(\bar{\Delta}).
\end{cases} \quad (7)$$

Now, guided by our content-aware visual salience measure, the error metric can be weighted by the weight map $\varpi(\boldsymbol{v})$ which is derived from the mesh salience:

$$\text{Error}(\boldsymbol{v}) = (\varpi(\boldsymbol{v})\boldsymbol{A}(\bar{\boldsymbol{v}}), \varpi(\boldsymbol{v})\boldsymbol{b}(\bar{\boldsymbol{v}}), \varpi(\boldsymbol{v})c(\bar{\boldsymbol{v}})). \quad (8)$$

To preserve high saliency vertices with high contraction costs, the weight map $\varpi(\boldsymbol{v})$ can be specified as

$$\varpi(\boldsymbol{v}) = \begin{cases} \kappa s(\boldsymbol{v}), & \text{if } s(\boldsymbol{v}) - \bar{s} > \lambda\sigma_s, \\ s(\boldsymbol{v}), & \text{otherwise.} \end{cases} \quad (9)$$

Here $s(\boldsymbol{v})$ is our estimated salience measure of vertex $\boldsymbol{v}$, and $\bar{s}$ and $\sigma_s$ denote the mean and standard deviation of salience distribution $s(\boldsymbol{v})$, respectively. In our practice, we use $\kappa$=50.0 and $\lambda$=1.33.

During the vertex pair collapse procedure ordered by increasing the error cost, the weighted quadric error metric for each potential vertex pair ($\boldsymbol{v}_i$, $\boldsymbol{v}_j$) can be calculated by adding the quadrics of their end vertices:

$$\text{Error}(\boldsymbol{v}_i, \boldsymbol{v}_j) = \big(\varpi(\boldsymbol{v}_i)\boldsymbol{A}(\bar{\boldsymbol{v}}_i) + \varpi(\boldsymbol{v}_j)\boldsymbol{A}(\bar{\boldsymbol{v}}_j), \varpi(\boldsymbol{v}_i)\boldsymbol{b}(\bar{\boldsymbol{v}}_i) + \varpi(\boldsymbol{v}_j)\boldsymbol{b}(\bar{\boldsymbol{v}}_j), \varpi(\boldsymbol{v}_i)c(\bar{\boldsymbol{v}}_i) + \varpi(\boldsymbol{v}_j)c(\bar{\boldsymbol{v}}_j)\big). \quad (10)$$

The optimal contraction point $\boldsymbol{v}^*$ for vertex pair ($\boldsymbol{v}_i$, $\boldsymbol{v}_j$) can be determined by minimizing the quadric error cost Error($\boldsymbol{v}_i$, $\boldsymbol{v}_j$) given in Eq. (10). Similar to Lee *et al.* (2005), if vertex pair ($\boldsymbol{v}_i$, $\boldsymbol{v}_j$) is contracted as a new point $\boldsymbol{v}^*$, the weight of contracted point $\boldsymbol{v}^*$ can be updated as $\varpi(\boldsymbol{v}^*) = \varpi(\boldsymbol{v}_i) + \varpi(\boldsymbol{v}_j)$. The weighted quadric error metric of point $\boldsymbol{v}^*$ can thus be simply computed as

$$\text{Error}(\boldsymbol{v}^*) = \big(\varpi(\boldsymbol{v}^*)(\boldsymbol{A}(\bar{\boldsymbol{v}}_i) + \boldsymbol{A}(\bar{\boldsymbol{v}}_j)), \varpi(\boldsymbol{v}^*)(\boldsymbol{b}(\bar{\boldsymbol{v}}_i) + \boldsymbol{b}(\bar{\boldsymbol{v}}_j)), \varpi(\boldsymbol{v}^*)(c(\bar{\boldsymbol{v}}_i) + c(\bar{\boldsymbol{v}}_j))\big). \quad (11)$$

For each pair contraction ($\boldsymbol{v}_i$, $\boldsymbol{v}_j$)→$\boldsymbol{v}^*$, a small group of vertices adjacent to vertex $\boldsymbol{v}_i$ or vertex $\boldsymbol{v}_j$ should be connected with a new point $\boldsymbol{v}^*$, and the error cost for these pairs should also be updated.

Finally, using a heap keyed on cost with the minimum weighted quadric error cost pair at the top, our visual salience guided shape simplification scheme will iteratively contract vertex pairs of least weighted quadric error cost from the heap until the simplification rate defined by the user is achieved.

## 5 Experimental results

The proposed visual salience guided shape simplification algorithm has been implemented on a PC with a Pentium IV 3.0 GHz CPU, 1 GB memory. As a preprocessing step, based on the relief height distribution, the content-aware salience map is extracted for the underlying complex model. Guided by our salience measure, our feature-aware shape simplification scheme is robust and effective for various 3D complex shapes.

### 5.1 Feature-aware adaptive simplification

By incorporating the content-aware visual salience measure into the re-sampling operation, our adaptive feature-aware shape simplification approach can be performed by vertex pair collapse, which makes the simplified model closer to the original one by adopting our salience-weighted quadric error metric defined in a high-dimensional feature space to measure the edge collapse error.

Fig. 4 shows the results of our salience guided feature-aware shape simplification for the Horse model and Lion model. Figs. 4b–4d are the re-sampling results obtained using our salience guided simplification scheme with the simplification rate 80.0%, 90.0%, 95.0%, respectively. Our experimental results strongly demonstrate the great adaptability of our shape simplification scheme to the visually salient features of the underlying meshes. The sampled vertices of the final simplified model are dense in the visually salient feature regions, whereas they are sparse in the visually less salient regions or relatively planar regions.

To evaluate the simplification quality generated by our feature-aware re-sampling algorithm, similar to the tool Metro (Cignoni *et al.*, 1998; Miao *et al.*, 2012a), we measure the normalized maximum geometric error (Eq. (12)) and the normalized root mean square (RMS) error (Eq. (13)) between the original mesh $S$ and the simplified version $S'$, that is,

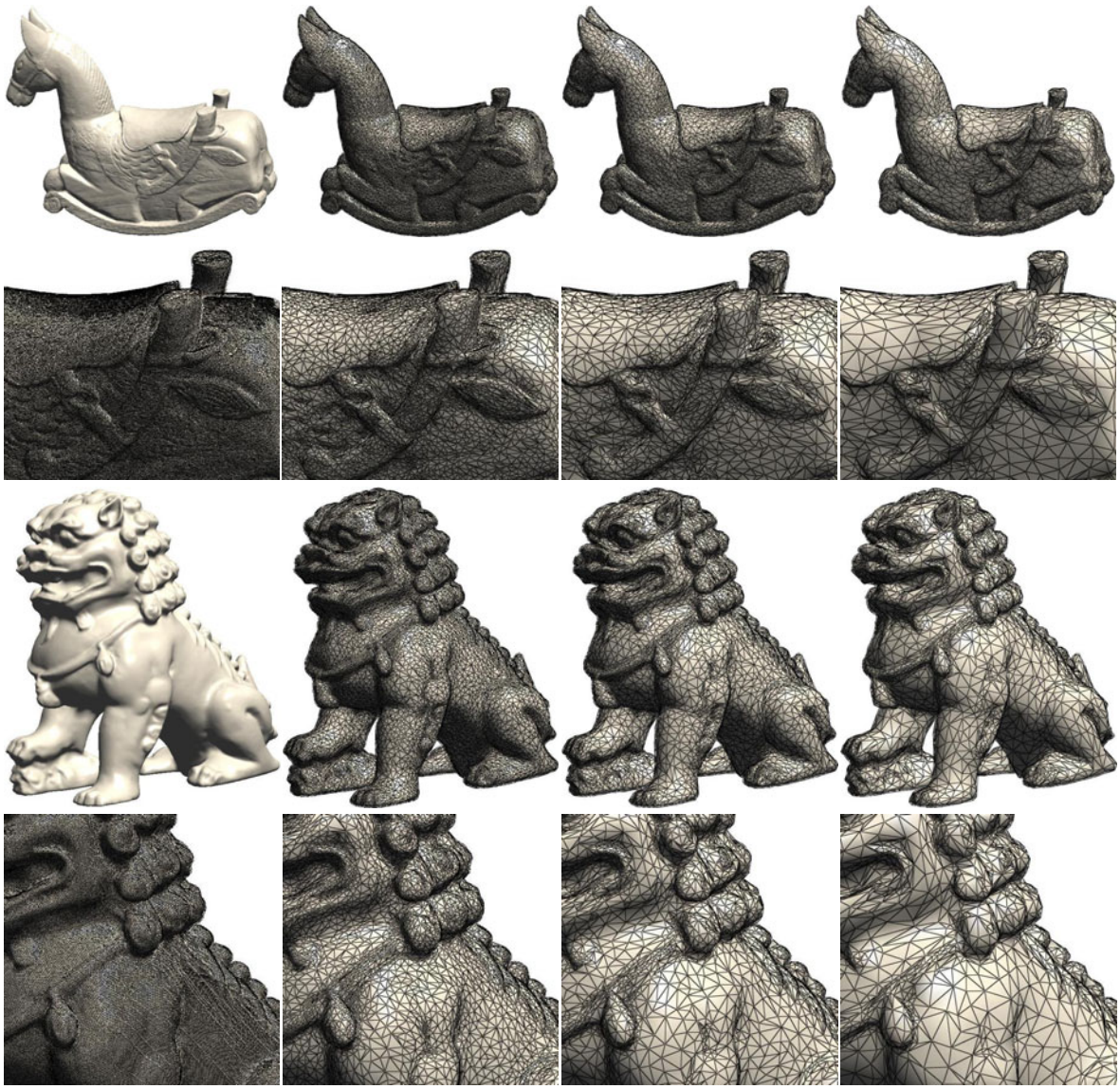


**Fig. 4 Feature-aware simplification for the Horse model and Lion model**

(a) Original models; (b, c, d) The re-sampling results obtained using our salience guided feature-aware simplification scheme with the simplification rate 80.0%, 90.0%, 95.0%, respectively

$$\Delta^*_{\max}(S, S') = \frac{\max_{v \in S} d(\boldsymbol{v}, S')}{\text{bb\_diag}}, \quad (12)$$

$$\Delta^*_{\text{RMS}}(S, S') = \frac{1}{\text{bb\_diag}} \sqrt{\frac{1}{|S|} \sum_{v \in S} d^2(\boldsymbol{v}, S')}. \quad (13)$$

Here, the geometric distance error $d(\boldsymbol{v}, S')$ means the minimum Euclidean distance between vertex $\boldsymbol{v} \in S$ and the simplified surface $S'$, which is approximated by the minimum distance of the vertex to the discrete surface sampling point sets on the simplified surface. The scale bb_diag is the diagonal length of the bounding box for the underlying model. Note that the simplification rate can be easily given by the user, and that the geometric error between the original and simplified versions of the underlying model can be estimated directly.

Table 1 shows the performance data and geometric error statistics for re-sampling of different models. The quantitative error estimates, i.e., the

**Table 1 Performance data and error statistics of different models at the simplification rate of 80.0%, 90.0%, or 95.0%**

| Model | Number of original vertices | Number of simplified vertices | | | Maximum error | | | RMS error | | |
|---|---|---|---|---|---|---|---|---|---|---|
| | | 80.0% | 90.0% | 95.0% | 80.0% | 90.0% | 95.0% | 80.0% | 90.0% | 95.0% |
| Blade | 195 156 | 39 031 | 19 515 | 9757 | 0.0041 | 0.0055 | 0.0075 | 0.0009 | 0.0011 | 0.0021 |
| Lion | 152 807 | 30 561 | 15 280 | 7640 | 0.0060 | 0.0086 | 0.0130 | 0.0015 | 0.0023 | 0.0034 |
| Mountain | 131 584 | 26 316 | 13 158 | 6579 | 0.0050 | 0.0094 | 0.0112 | 0.0010 | 0.0015 | 0.0022 |
| Horse | 117 690 | 23 537 | 11 769 | 5884 | 0.0053 | 0.0076 | 0.0096 | 0.0013 | 0.0019 | 0.0028 |
| Bunny | 72 027 | 14 405 | 7202 | 3601 | 0.0069 | 0.0088 | 0.0124 | 0.0018 | 0.0026 | 0.0038 |
| Hand | 53 054 | 10 610 | 5305 | 2652 | 0.0071 | 0.0088 | 0.0183 | 0.0019 | 0.0029 | 0.0043 |

normalized maximum geometric error and normalized root mean square (RMS) error, are listed for each mesh model with the simplification rate 80.0%, 90.0%, 95.0%, respectively. For example, the total number of vertices of the original Lion model is 152 807, and thus it will be simplified to 20.0% (the number of vertices of the simplified model is 30 561), 10.0% (the number of vertices of the simplified model is 15 280), and 5.0% (the number of vertices of the simplified model is 7640) for the simplification rate 80.0%, 90.0%, 95.0%, respectively. Using our salience guided feature-aware simplification scheme, the normalized maximum geometric error is 0.0060 and the normalized RMS error is 0.0015 with the simplification rate 80.0%; when the simplification rate is increased to 90.0%, the normalized maximum geometric error and normalized RMS error become 0.0086 and 0.0023, respectively. Furthermore, if the simplification rate is increased to 95.0%, the normalized maximum geometric error and normalized RMS error are 0.0130 and 0.0034, respectively. Experimental results show that the increased simplification rate always leads to a lower number of sampled vertices in the final simplified model but a higher geometric error, as expected.

### 5.2 Comparisons with different simplification schemes

Essentially, our feature-aware simplification scheme re-samples the given 3D model by iterative contractions of vertex pairs, and tracks the approximate error during the simplification operation. Thus, for uniformity, we compare our scheme with only quadric error metric based simplification approaches for 3D meshes. The traditional QSlim approach proposed by Garland and Heckbert (1997) is a pure geometry-based mesh simplification algorithm. However, our shape simplification method will re-sample the underlying shape in a feature-aware manner by weighting the high-dimensional feature space quadric error metric of vertex pair contractions with the visually perceptual measure. We compare our salience guided simplification approach with the traditional QSlim simplification method (Garland and Heckbert, 1997) for the Blade model and Stanford Bunny model, respectively (Fig. 5). Here, for the Blade model (the total number of vertices of the original model is 195 156), it has been simplified to 10.0% of the original vertices. For the Stanford Bunny model (the total number of vertices of the original model is 72 027), it has been simplified to 20.0% of the original vertices. The adaptive vertex distribution of the final simplified models generated by our feature-aware simplification scheme (Fig. 5) accounts for the salient features and thus yields better visual fidelity; that is, the vertices of simplified models are dense in the regions of salient features and comparatively sparse in the non-feature regions.

Moreover, Fig. 6 gives the results of using our salience guided re-sampling scheme with different salience maps for the Hand model. The total number of vertices of the original Hand model is 53 054, and it has been simplified to 10.0% of the original vertices. As shown in Fig. 6, the vertex adaptive distribution of the final simplified models is also affected by different salience definitions. Compared with the salience guided re-sampling scheme using Lee *et al.* (2005) and Liu *et al.* (2007)'s mesh salience maps, the vertex distribution of the final model using our content-aware salience map effectively reflects the visually salient features of underlying relief shapes and thus yields better visual fidelity.

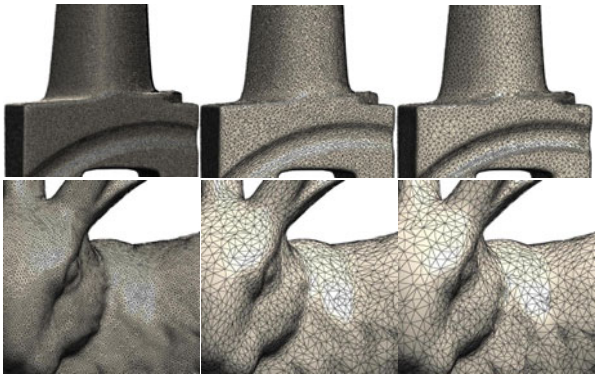


**Fig. 5 Comparison with the QSlim approach (Garland and Heckbert, 1997) for the Blade model and Stanford Bunny model**

(a) Zoom-in view of the original models; (b) Simplification results using the QSlim approach; (c) Simplification results using our approach

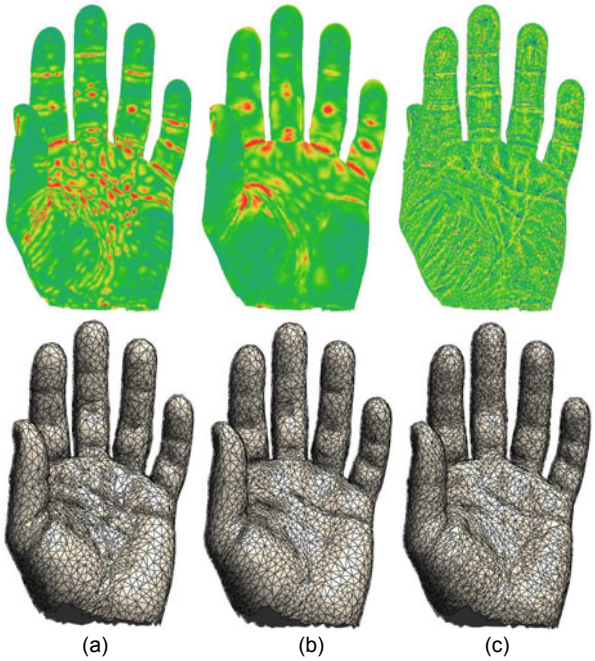


**Fig. 6 Comparison of our salience guided simplification scheme using different salience maps for the Hand model**

(a) Our content-aware salience map and the salience guided simplification result; (b) Lee *et al.* (2005)'s salience map and the salience guided simplification result; (c) Liu *et al.* (2007)'s salience map and the salience guided simplification result

## 6 Conclusions

In this paper, by incorporating the content-aware visual salience measure of 3D shapes into the re-sampling operation, a feature-aware simplification technique is presented for polygonal meshes. To yield better visual performance for simplified models, our content-aware visual salience measure is calculated using a center-surround operator on Gaussian-weighted relief heights in a multi-scale bottom-up manner. Guided by the visual salience map, our shape simplification scheme can be performed by exploiting the visual salience weighted quadric error metric defined in a high-dimensional feature space to measure the vertex pair collapse error. The feature space quadric error metric is computed in a 6D space by combining the position and normal information of mesh vertices. Experimental results show that our salience guided simplification scheme adaptively and effectively re-samples the given models and always accounts for the visually salient features of complex shapes.

In the future, due to our content-aware visual salience measure, we will develop some related techniques about perceptually driven 3D shape modeling and rendering, such as visual salience guided viewpoint selection and salience-based shape abstraction.

## References

Botsch, M., Pauly, M., Kobbelt, L., *et al*., 2007. Geometric modeling based on polygonal meshes. ACM SIGGRAPH, Course Notes, Article 1. [doi:10.1145/1281500.1281640]

Cignoni, P., Rocchini, C., Scopigno, R., 1998. Metro: measuring error on simplified surfaces. *Comput. Graph. Forum*, **17**(2):167-174. [doi:10.1111/1467-8659.00236]

Cohen, J., Varshney, A., Manocha, D., *et al*., 1996. Simplification envelopes. Proc. 23rd Annual Conf. on Computer Graphics and Interactive Techniques, p.119-128. [doi:10.1145/237170.237220]

Corsini, M., Larabi, M.C., Lavoué, G., *et al*., 2013. Perceptual metrics for static and dynamic triangle meshes. *Comput. Graph. Forum*, **32**(1):101-125. [doi:10.1111/cgf.12001]

Fleming, R.W., Singh, M., 2009. Visual perception of 3D shape. ACM SIGGRAPH, Course Notes, Article 24. [doi:10.1145/1667239.1667263]

Garland, M., Heckbert, P.S., 1997. Surface simplification using quadric error metrics. Proc. 24th Annual Conf. on Computer Graphics and Interactive Techniques, p.209-216. [doi:10.1145/258734.258849]

Garland, M., Heckbert, P.S., 1998. Simplifying surfaces with color and texture using quadric error metrics. Proc. IEEE Visualization, p.263-269.

Hoppe, H., 1996. Progressive meshes. Proc. 23rd Annual Conf. on Computer Graphics and Interactive Techniques, p.99-108. [doi:10.1145/237170.237216]

Hoppe, H., 1999. New quadric metric for simplifying meshes with appearance attributes. Proc. IEEE Visualization, p.59-66. [doi:10.1109/VISUAL.1999.809869]

Hoppe, H., DeRose, T., Duchamp, T., *et al*., 1993. Mesh optimization. Proc. 20th Annual Conf. on Computer Graphics and Interactive Techniques, p.19-26. [doi:10.1145/166117.166119]

Howlett, S., Hamill, J., O′Sullivan, C., 2005. Predicting and evaluating saliency for simplified polygonal models. *ACM Trans. Appl. Percept.*, **2**(3):286-308. [doi:10.1145/1077399.1077406]

Itti, L., Koch, C., Niebur, E., 1998. A model of saliency-based visual attention for rapid scene analysis. *IEEE Trans. Patt. Anal. Mach. Intell.*, **20**(11):1254-1259. [doi:10.1109/34.730558]

Lee, C.H., Varshney, A., Jacobs, D.W., 2005. Mesh saliency. *ACM Trans. Graph.*, **24**(3):659-666. [doi:10.1145/1073204.1073244]

Liu, Y., Liu, M., Kihara, D., *et al*., 2007. Salient critical points for meshes. Proc. ACM Symp. on Solid and Physical Modeling, p.277-282. [doi:10.1145/1236246.1236285]

Luebke, D., 2001. A developer's survey of polygonal simplification algorithms. *IEEE Comput. Graph. Appl.*, **21**(1):24-35. [doi:10.1109/38.920624]

Luebke, D., Hallen, B., 2001. Perceptually driven simplification for interactive rendering. Proc. 12th Eurographics Workshop on Rendering, p.223-234. [doi:10.2312/EGWR/EGWR01/223-234]

Luebke, D., Reddy, M., Cohen, J.D., *et al*., 2003. Level of detail for 3D graphics. Morgan Kaufman Publishers, San Francisco, CA, USA.

Miao, Y., Bösch, J., Pajarola, R., *et al*., 2012a. Feature sensitive re-sampling of point set surfaces with Gaussian spheres. *Sci. China Inform. Sci.*, **55**(9):2075-2089. [doi:10.1007/s11432-012-4637-0]

Miao, Y., Feng, J., Wang, J., *et al*., 2012b. A multi-channel salience based detail exaggeration technique for 3D relief surfaces. *J. Comput. Sci. Technol.*, **27**(6):1100-1109. [doi:10.1007/s11390-012-1288-y]

Ohtake, Y., Belyaev, A., Seidel, H.P., 2002. Mesh smoothing by adaptive and anisotropic Gaussian filter applied to mesh normals. Proc. Vision, Modeling and Visualization, p.203-210.

Press, W.H., Teukolsky, S.A., Vetterling, W.T., *et al*., 1992. Numerical Recipes in C: the Art of Scientific Computing (2nd Ed.). Cambridge University Press, New York.

Qu, L., Meyer, G.W., 2008. Perceptually guided polygon reduction. *IEEE Trans. Visual. Comput. Graph.*, **14**(5):1015-1029. [doi:10.1109/TVCG.2008.51]

Shilane, P., Funkhouser, T., 2007. Distinctive regions of 3D surfaces. *ACM Trans. Graph.*, **26**(2):7:1-7:15. [doi:10.1145/1243980.1243981]

Todd, J.T., 2004. The visual perception of 3D shape. *Trends Cogn. Sci.*, **8**(3):115-121. [doi:10.1016/j.tics.2004.01.006]

van Kaick, M., Pedrini, H., 2006. A comparative evaluation of metrics for fast mesh simplification. *Comput. Graph. Forum*, **25**(2):197-210. [doi:10.1111/j.1467-8659.2006.00935.x]

Wei, J., Lou, Y., 2010. Feature preserving mesh simplification using feature sensitive metric. *J. Comput. Sci. Technol.*, **25**(3):595-605. [doi:10.1007/s11390-010-9348-7]

Williams, N., Luebke, D., Cohen, J.D., *et al*., 2003. Perceptually guided simplification of lit, textured meshes. Proc. Symp. on Interactive 3D Graphics, p.113-121. [doi:10.1145/641480.641503]

Wu, Y., He, Y., Cai, H., 2004. QEM-based mesh simplification with global geometry features preserved. Proc. 2nd Int. Conf. on Computer Graphics and Interactive Techniques in Australasia and South East Asia, p.50-57. [doi:10.1145/988834.988843]

Xiao, C., Fu, H., Tai, C.L., 2009. Hierarchical aggregation for efficient shape extraction. *Vis. Comput.*, **25**(3):267-278. [doi:10.1007/s00371-008-0226-z]

Xing, L.P., Hui, K.C., 2012. A visual and geometry-based hybrid approach for surface simplification. *Comput.-Aid. Des. Appl.*, **9**(2):167-176. [doi:10.3722/cadaps.2012.167-176]

Zatzarinni, R., Tal, A., Shamir, A., 2009. Relief analysis and extraction. *ACM Trans. Graph.*, **28**(5):136:1-136:7. [doi:10.1145/1618452.1618482]